COMPARISON BETWEEN SEVERAL PARAMETERIZATION SCHEMES IN WRF FOR SOLAR FORECASTING IN COASTAL ZONES

Israel López-Coto
Juan L. Bosch
Patrick Mathiensen
Jan Kleissl
Department of Mechanical and Aerospace Engineering
Center for Renewable Resources and Integration
University of California, San Diego
La Jolla, California 92093-0411
ilc@ucsd.edu
jlbosch@ucsd.edu
pmathies@ucsd.edu
jkleissl@ucsd.edu

ABSTRACT

The numerical weather prediction (NWP) models have widely demonstrated their usefulness in solar energy forecasting. Nevertheless, the high resolution and accuracy needed today for the operational management of solar resources necessitates a constant development of such models and a continuous effort in the accurately representation of the physical processes involved.

In coastal California, the principal source of NWP model inaccuracy is the presence of marine stratocumulus clouds. These clouds have a strong influence on the radiative balance and solar irradiance at the surface. In this work, the effect that several combinations of parameterization schemes have on simulating marine stratocumulus clouds is examined. Specifically, the cloud microphysics, cumulus, radiation and planetary boundary layer parameterization schemes implemented in the Weather Research and Forecasting Model (WRF) are analyzed. Additionally, the influence of the initial and boundary conditions in the model have been tested.

In order to quantify the overall model performance, WRF-simulated cloud water path was compared to MODIS cloud data, WRF-simulated GHI was compared to SolarAnywhere data, and WRF-simulated vertical temperature/mixing ratio profiles were compared against atmospheric radiosondes.

In general, the results revealed that the choice of parameterization in addition to the initialization dataset strongly influence the accuracy of the simulated cloud fields, the thermodynamic properties of the atmosphere, and the solar radiation reaching the surface.

1. INTRODUCTION

The principal factor limiting the extended applicability of renewable based energy is power output variability. Specifically, the solar energy is strongly affected by the presence of clouds, which cause strong spatio-temporal variability of the solar radiation reaching the surface. In southern California, marine layer cloud cover is common (1). Marine layer clouds are low-altitude stratocumulus clouds that are common in summer mornings. Generally these clouds are optically thick and can reduce photo-voltaic production by up to 70%.

Several methods of solar forecasting have been developed to accurately predict irradiance. For very short-term forecasting, statistical techniques based on analyses of historical irradiance time series are commonly used, (2, 3). Alternatively, imagery-based cloud advection techniques using local sky imagery (4) or satellite images (5) have been implemented. However, for longer forecast horizons (greater than 5 hours), physics-based weather models (numerical weather prediction (NWP)) are generally the most accurate method (5). Since NWP directly simulate the atmospheric thermodynamics that govern cloud cover, cloud formation and dissipation is intrinsically predicted and solar irradiance accuracy improved. Previous studies, however (6, 7, 8), have demonstrated that irradiance forecasts using the operational NWP are systematically erroneous and, thus, their applicability for

solar forecasting limited.

The principal sources of error in the NWP are the unresolved physical processes which are parameterized, the nonlinear interactions between the physical parameterizations, and errors in the initial conditions. Additionally, numerical diffusion and the horizontal and vertical resolution influence model accuracy. The principal aim of this work is to analyze the response of a high-resolution regional weather forecasting model (WRF) using several physical parameterizations and the effect of using different input data sources.

2. METHODS

2.1 WRF CONFIGURATION

The Weather Research and Forecasting Model (WRF) is the state of the art of Numerical Weather Prediction models. The Advanced Research WRF (ARW) core also known as Mass core, uses fully compressible, non-hydrostatic Eulerian equations on an Arakawa C-staggered grid with conservation of mass, momentum, entropy, and scalars (9).

In this work, the latest version WRFV3.4.1 has been used along with the IGBP-Modified MODIS 20-category Land Use dataset provided by the Boston University and modified by the NCEP.

A bidirectional strategy has been selected for downscaling the three selected domains which have 12, 4 and 1.3 km of horizontal resolution. These domains are centered in San Diego, California, (N32.881, W117.237) and they have 125 x 125, 124 x 124 and 100 x 100 horizontal grid cells respectively. Also, 75 vertical levels have been selected with higher resolution between the surface and 3 km.

The days 05/05/2011, 05/11/2011, 06/08/2011, 06/15/2011 and 06/23/2011 were selected because of marine layer conditions while 05/13/2011 was selected because the passing frontal system, (figure 1).

2.1.1 ENSEMBLE MEMBERS

A set of high-resolution model simulations was conducted using 4 microphysics, 2 cumulus, 4 radiation, 2 PBL schemes and 2 soil models, table 1. This results in 72 combinations of WRF physic parameterizations forming the ensemble.

In this study, the ensemble members are named using letters and numbers combination which are representative of the physical options that were used. The letters refer to the scheme type and the number to the WRF namelist option. The soil model label is included in the name for some schemes. In cases when it is not, the Noah soil model is used by default. For example, a member named P5M10C1S4 was simulated using the MYNN planetary boundary layer (PBL) scheme, the Thompson microphysics (MP) scheme, the Kain-Fritsch cumulus (CU) scheme, the RRTMG short and long wave radiation scheme (SW/LW) and the Noah soil model.

The simulations had a maximum forecast run time of 36 hours, beginning at 12:00 UTC for the day 08/06/2011 along with the North American Regional Reanalysis (NARR) data, provided by the National Centers for Environmental Prediction (NCEP), as boundary and initial conditions.

2.1.2 SELECTED SCHEMES

After the initial global ensemble was analyzed, 9 schemes were selected and 5 new days were simulated in order to test the behavior for different meteorological conditions. The days 05/05/2011, 05/11/2011, 06/15/2011 and 06/23/2011 were selected because of marine layer conditions while 05/13/2011 was selected because the passing frontal system.

The simulations were conducted using NARR as boundary and initial conditions. However, a extra member has been added to the simulation which use the configuration P5M8C1S1 and the NCEP North American Model (NAM) data as boundary and initial conditions.

2.2 OBSERVATIONAL DATA SOURCES

SolarAnywhere (SAW) data are derived from Geostationary Operational Environmental Satellite (GOES) visible imagery (24). SAW calculates global horizontal irradiance (GHI) using the SUNY model. To obtain GHI, a cloud index is calculated for each pixel from the reflectance measured by the satellite. Instantaneous, spatially averaged GHI is then calculated by using the cloud index along with a clear sky model that considers local and seasonal effects of turbidity (25). SAW enhanced resolution satellite-derived irradiation with 30-min temporal and 1 km spatial resolutions is applied in this study.

MODIS Level2 Cloud Water Path (CWP) and the associated uncertainty data are used to compare against WRF-simulated cloud cover. MODIS (or Moderate Resolution Imaging Spectroradiometer) is a key instrument aboard the Terra (EOS AM) and Aqua (EOS PM) satellites. Terra's orbit around the Earth is timed so that it passes from north to south across the equator in the morning, while Aqua passes south to north over the equator in the afternoon. Terra MODIS and Aqua MODIS are viewing the entire Earth's surface every 1 to 2 days, acquiring data in 36 spectral bands. The MODIS

Cloud Product combines infrared and visible techniques to determine both physical and radiative cloud properties with a horizontal resolution of ~1 km (26, 27).

Lastly, from MCAS Miramar, San Diego, (KNKX, N32.85, W117.11) radiosonde data was obtained from the Integrated Global Radiosonde Archive (IGRA) (28). This includes profiles of temperature and mixing ratio. Additionally, the inversion base height is calculated based on the criterion of environmental lapse rate > 0.

2.3 ERROR METRICS

In this study, the well-known mean difference (BIAS) and the root mean square deviation (RMSD) were used. The observational fields were interpolated in order to match the WRF inner domain resolution using bivariate linear interpolation. The BIAS and the RMSD have been calculated across the inner domain per each available time.

$$\Delta_i = x_i - x_i^{Ref} \quad (1)$$

$$BIAS = \frac{1}{N}\sum_{i=1}^{N}\Delta_i \quad (2)$$

$$RMSD = \sqrt{\frac{1}{N}\sum_{i=1}^{N}\Delta_i^2} \quad (3)$$

In the case of MODIS comparison, a weight factor was applied in order to take into account the uncertainty of the observed Cloud Water Path. This weight function (w) was defined as a linear function of the relative error (e) per pixel and it is written as follows:

$$\omega_i = \begin{cases} 1 - e_i & ; \ e_i \in [0,1] \\ 0 & ; \ e_i \notin [0,1] \end{cases} \quad (4)$$

$$\Delta_i = (x_i - x_i^{Ref}) \cdot \omega_i \quad (5)$$

The mean difference and the root square deviation obtained using this weight function are called as wBIAS and wRMSD in the text.

With this, we derived the BIAS and RMSD temporal evolution during daytime by comparing with SAW data with a temporal resolution of half an hour. Based on the BIAS evolution, an agglomerative hierarchical clustering method (29, 30, 31) was applied in order to determine the schemes which present the higher behavior similarities.

The selected comparison metric has been the Euclidean distance between elements, defined as:

$$\|\boldsymbol{x} - \boldsymbol{y}\| = \sqrt{\sum_{i=1}^{N}(x_i - y_i)^2} \quad (6)$$

The linkage criterion selected was the “complete” criterion, which is based on the max distance between pairs.

The number of cluster selected has been based on the variability generated by each cluster reaching a compromise between low standard deviation per cluster and low number of clusters.

3. RESULTS

3.1 GLOBAL ENSEMBLE

Based on the SAW-derived BIAS daytime evolution, we applied an agglomerative hierarchical clustering method in order to determine the similarities between model parameterizations, (figure 2).

The least important physic parameterizations generating variability in the results was the microphysics scheme. Next were the soil model and the PBL scheme. In the contrary, the most important parameterization was the radiation scheme as it controls the energy budget.

Next, the number of clusters was selected based on the variability generated by each cluster, eventually reaching a compromise between low standard deviation per cluster and low number of clusters, (figure 3).

As can be seen in the figure, the standard deviation presented for each group is reduced as the number of clusters increases. However, a good compromise between the number of clusters and variability could be reached by selecting a number as low as 8 clusters.

In general, all the schemes show a GHI overestimation throughout the day. However, the clusters 5, 7 and 8 underestimate the GHI in the afternoon, the magnitude of which is strongest for cluster 7 which contains only 3 members.

The highest bias is observed in general around 10:00 PST, being largest for the cluster 2 and lowest for the cluster 7. However, the most accurate morning evolution is obtained for the cluster 8, which shows an almost constant BIAS around 50 Wm^{-2} until 9:00 PST

3.2 SELECTED SCHEMES

After clustering results, we have selected a representative member per cluster (shown in Table 2) in order to cover the whole model variability and to analyze the model behavior under different meteorological conditions.

In general, all the schemes show similar bias evolutions, with higher BIAS in the mornings and lower in the afternoon, (figure 4). However, some of the model configurations maintain positive BIAS for nearly all days while others show negative BIAS in the afternoon for 2 or 3 days depending on the scheme.

The days 06/15/2011 and 06/15/2011 show almost the same trend for all of the schemes, reaching higher values for P5M10C14S5 and P5M10C1S5.

The best simulated day is the 05/05/2011 for all of the schemes. However, this day shows a different evolution during the afternoon for the schemes P5M8C14S5, P5M10C14S5 and P5M10C1S5 where the minimum BIAS is obtained around 16:00 PST instead at noon. Additionally, this behavior is observed for all of the schemes during the day05/11/2011 .

The weighed BIAS and RMSD derived from MODIS Cloud Water Path are show in the tables 3 and 4. The proper simulation of the cloud water path is critical in determining the radiation attenuated by the clouds. As can be seen, the input data have an important effect on the model behavior since the day 05/13/2011 shows very high values for the model runs with NARR. However, the results are comparable for the rest of the days.

The lowest wRMSD are observed for the days 05/05/2011 and 05/11/2011 and also the wBIAS are close to zero for these days. For the days 06/15/2011 and 06/23/2011, negative wBIAS is observed indicating the model is underestimating the cloud water content. These two days present very similar values for the both score functions, indicating the meteorological forcing is too strong to be affected by the model configuration selected.

In the tables 5 and 6, the BIAS and RMSD derived from radiosondes are given. In general, all of the schemes underestimate the profile temperature for all days and the mixing ratio for four of the six days. Also, the new SAS cumulus scheme (C14) is increasing slightly the amount of water in the column. However, the amount is comparable for all of the schemes indicating small differences in the vertical profile could derive in large global evolution discrepancies.

Table 7 presents the differences between the inversion height derived from the model simulations and the observed radiosondes. As can be seen, the PBL and the radiation schemes are affecting the inversion base height. The days 2011/05/14, 2011/06/09 and the 2011/06/15 show the same tendency for all of the schemes, being negative (height underestimation) for the first two and positive for the last one.

Additionally, the YSU (P1) configurations provide higher inversion heights than the MYNN (P5) ones. However, the MYNN containing configurations trend to provide too low inversion base which is partially corrected by the inclusion of the RRMTG radiation scheme (S4), probably due to a lower radiation attenuation from clouds and, thus, a higher surface temperature which increases the surface heat flux.

Alternatively, the day 06/16/2011 shows a general overestimation of the inversion base height which could be due to the input data. This fact again would indicate that the input data are strongly forcing the results.

4. CONCLUSIONS

In this work, the capability of several combinations of cloud microphysics, cumulus, radiation and planetary boundary layer parameterization schemes implemented in the Weather Research and Forecasting Model (WRF) to simulate accurately the marine stratocumulus in the California coast were analyzed. Additionally, the influence of the initial and boundary conditions in the model have been tested.

A set of high-resolution model simulations was conducted using 4 microphysics, 2 cumulus, 4 radiation, 2 PBL schemes and 2 soil models. With this, we selected 72 combinations of WRF physic parameterizations and compared the results to cloud data from MODIS, SolarAnywhere data from the SUNY model, and temperature and mixing ratio profiles provided by radiosondes.

After the initial global ensemble was analyzed by means of agglomerative hierarchical clustering, 9 schemes were selected and 5 new days were simulated in order to test the behavior for different meteorological conditions.

The results showed that the least influential physics parameterization is the microphysics scheme. This is followed by the soil model and the PBL scheme. On the contrary, the most important parameterization causing variability is the radiation scheme as it controls the energy budget.

In general, all the schemes show a GHI overestimation during the whole day, with the largest magnitudes around

10:00 PST. However, some schemes underestimate the GHI in the afternoon.

The input data (initial and boundary conditions) have an important effect on the model behavior. However, the results are comparable in general for NARR and NAM for the majority of the days.

Additionally, some days present very similar values for the score functions, indicating the meteorological forcing is too strong or the errors in the initial conditions are too large to be effected by the model configuration selected.

In general, all of the schemes are underestimating the temperature profile for all days and the mixing ratio for four of the six days. Also, the new SAS cumulus scheme (C14) slightly increases the amount of water in the column. However, the amount is comparable for all of the schemes indicating small differences in the vertical profile could result in large global evolution discrepancies.

Finally, the PBL and the radiation schemes affect the inversion base height. The YSU containing configurations tend to simulate higher inversion heights than the MYNN containing configurations. However, the MYNN simulate too low of inversion bases which is partially corrected by the inclusion of the RRTMG radiation scheme. This is probably due to a lower radiation attenuation from clouds and, thus, a higher surface temperature which increase the surface heat flux.

REFERENCES

(1) Blake, D., (1928). Temperature inversions at San Diego, as deduced from aerographical observations by airplane. Monthly Weather Review. 56, 221-224.

(2) Marquez, R., and Coimbra, C., (2011). Forecasting of global and direct solar irradiance using stochastic learning methods, ground experiments and the NWS database. Solar Energy. 85(5), 746-756.

(3) Coimbra, C., and Pedro, H., (2013). "Stochastic learning methods" in Solar Energy Forecasting and Resource Assessment. Ed: Jan Kleissl. Elsevier, 2013.

(4) Chow, C.W., Urquhart, B., Lave, M., Dominguez, A., Kleissl, J., Shields, J., and Washom, B., (2011). Intra-hour forecasting with a total sky imager at the UC San Diego solar energy testbed. Solar Energy. 85(11), 2881-2893.

(5) Perez, R., Kivalov, S., Schlemmer, J., Hemker, K., Renné, D., and Hoff, T., (2010). Validation of short and medium term operational solar radiation forecasts in the US. Solar Energy. 84(12), 2161-2172.

(6) Lorenz, E., Hurka, J., Heinemann, D., and Beyer, H., (2009). Irradiance forecasting for the power prediction of grid-connected photovoltaic systems. IEEE Journal of Selected Topics in Applied Earth Observations and Remote Sensing. 2(1), 2-10.

(7) Mathiesen, P., and Kleissl, J., (2011). Evaluation of numerical weather prediction for intra-day solar forecasting in the continental United States. Solar Energy. 85(5), 967-977.

(8) Mathiesen, P., Brown, J., and Kleissl, J., (2012). Geostrophic wind dependent probabilistic irradiance forecasts for coastal California. IEEE Transactions on Sustainable Energy. 99, 1-9.

(9) Skamarock, W. C., Klemp, J. B., Dudhia, J., Gill, D. O., Barker, D. M., Duda, M. G., Huang, X-Y., Wang, W., and Powers, J. G. (2008). A Description of the Advanced Research WRF Version 3, NCAR Technical Note, NCAR/TN–475+STR.

(10) Hong, S.-Y., and H.-L. Pan. (2006). Nonlocal boundary layer vertical diffusion in a medium-range forecast model, Mon. Wea. Rev., 124, 2322–2339.

(11) Nakanishi, M. and Niino, H., (2006). An Improved Mellor--Yamada Level-3 Model: Its Numerical Stability and Application to a Regional Prediction of Advection Fog, Boundary-Layer Meteorology, 119, 397-407.

(12) Lin, Y.-L., R. D. Farley, and H. D. Orville, (1983). Bulk parameterization of the snow field in a cloud model. J. Climate Appl. Meteor., 22, 1065–1092.

(13) Thompson, G., R. M. Rasmussen, and K. Manning, (2004). Explicit forecasts of winter precipitation using an improved bulk microphysics scheme. Part I: Description and sensitivity analysis. Mon. Wea. Rev., 132, 519–542.

(14) Morrison, H., J. A. Curry, and V. I. Khvorostyanov, (2005). A new double-moment microphysics parameterization for application in cloud and climate models, Part I: Description. J. Atmos. Sci., 62, 1665–1677.

(15) Lim, Kyo-Sun Sunny, Song-You Hong, (2010). Development of an Effective Double-Moment Cloud Microphysics Scheme with Prognostic Cloud Condensation Nuclei (CCN) for Weather and Climate Models. Mon. Wea. Rev., 138, 1587–1612.

(16) Kain, J. S., (2004). The Kain-Fritsch convective parameterization: An update. J. Appl. Meteor., 43, 170–

181.

(17) Han, J. and H.-L. Pan, (2010). Revision of Convection and Vertical Diffusion Schemes in the NCEP Global Forecast System, NCEP Office Note 464, 42pp.

(18) Dudhia, J., (1989). Numerical study of convection observed during the winter monsoon experiment using a mesoscale two-dimensional model, J. Atmos. Sci., 46, 3077−3107

(19) Mlawer, E. J., S. J. Taubman, P. D. Brown, et al., (1997). Radiative transfer for inhomogeneous atmosphere: RRTM, a validated correlated-k model for the longwave, J. Geophys. Res., 102(D14), 16663−16682

(20) Collins, W.D. et al., (2004). Description of the NCAR Community Atmosphere Model (CAM 3.0), NCAR Technical Note, NCAR/TN-464+STR, 226pp.

(21) Chou M.-D., and M. J. Suarez, (1994). An efficient thermal infrared radiation parameterization for use in general circulation models. NASA Tech. Memo. 104606, 3, 85pp.

(22) Chen, F., and J. Dudhia, (2001). Coupling an advanced land-surface/ hydrology model with the Penn State/ NCAR MM5 modeling system. Part I: Model description and implementation. Mon. Wea. Rev., 129, 569–585.

(23) Smirnova, T. G., J. M. Brown, and S. G. Benjamin, (1997). Performance of different soil model configurations in simulating ground surface temperature and surface fluxes. Mon. Wea. Rev., 125, 1870–1884.

(24) Perez R., P. Ineichen, K. Moore, M. Kmiecik, C. Chain,R. George and F. Vignola, (2002). A New Operational Satellite-to-Irradiance Model. Solar Energy 73, 5, pp.307-317

(25) Perez R., P. Ineichen, M. Kmiecik, K. Moore, R.George and D. Renne, (2004). Producing satellite-derived irradiances in complex arid terrain. SolarEnergy 77, 4, 363-370

(26) Baum, B.A. and S. Platnick, (2006). Introduction to MODIS cloud products. In Earth Science Satellite Remote Sensing, Vol. 1: Science and instruments. Edited by J. J. Qu et al., Springer-Verlag.

(27) King M. D., W. P. Menzel, Y. J. Kaufman, D. Tanré, B. C. Gao, S. Platnick, S. A. Ackerman, L.
A. Remer, R. Pincus, and P. A. Hubanks, (2003). Cloud, Aerosol and Water Vapor Properties from MODIS., IEEE Trans. Geosci. Remote Sens., 41, pp. 442-458

(28) Durre, I., Vose, R.S., Wuertz, D.B., (2006). Overview of the integrated global radiosonde archive. Journal of Climate 19, 53–68.

(29) Everitt, B. (1974). Cluster Analysis. London: Heinemann Educ. Books.

(30) Hartigan, J. A. (1975). Clustering Algorithms. New York: Wiley.

(31) Gordon, A. D. (1999). Classification. Second Edition. London: Chapman and Hall / CRC

FIGURES AND TABLES

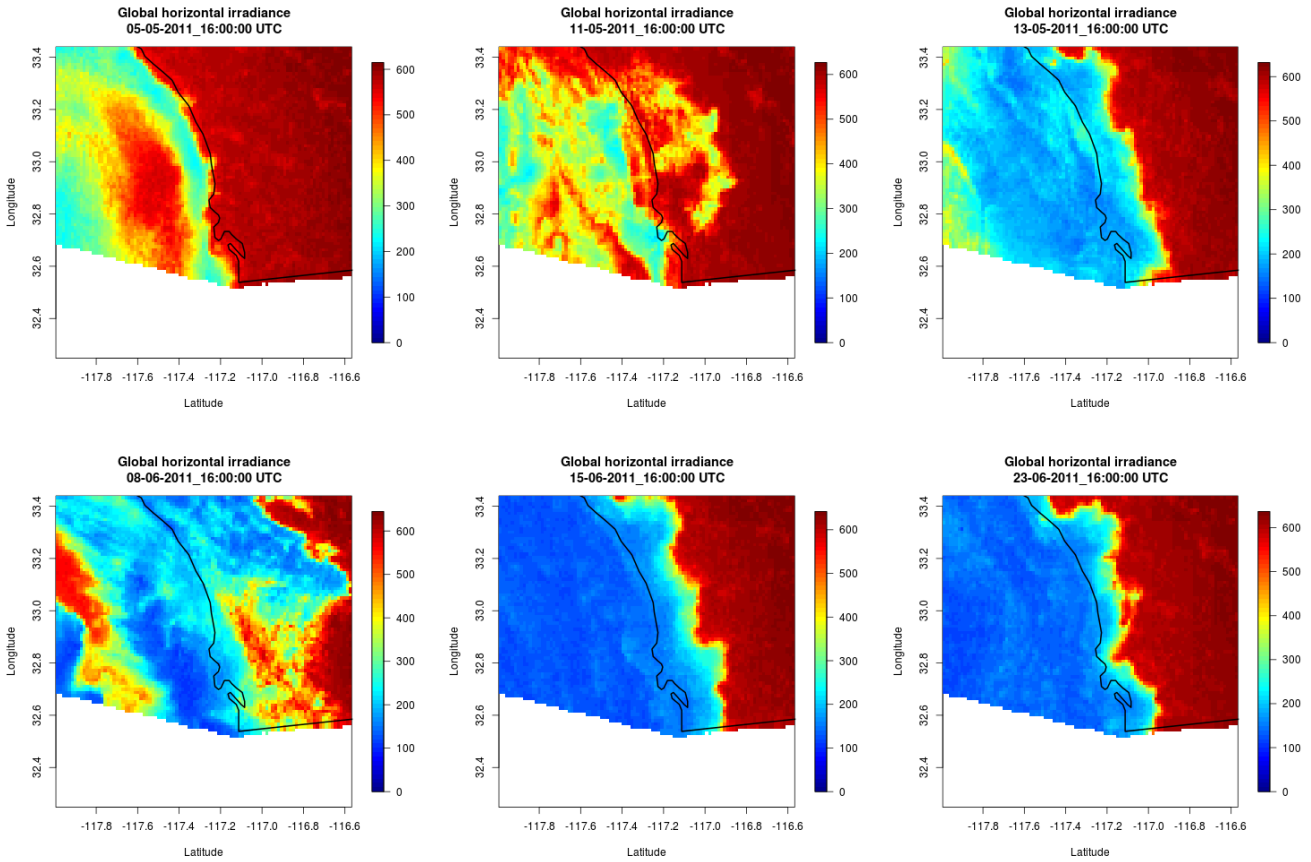

Figure 1. Global horizontal irradiance for the selected days

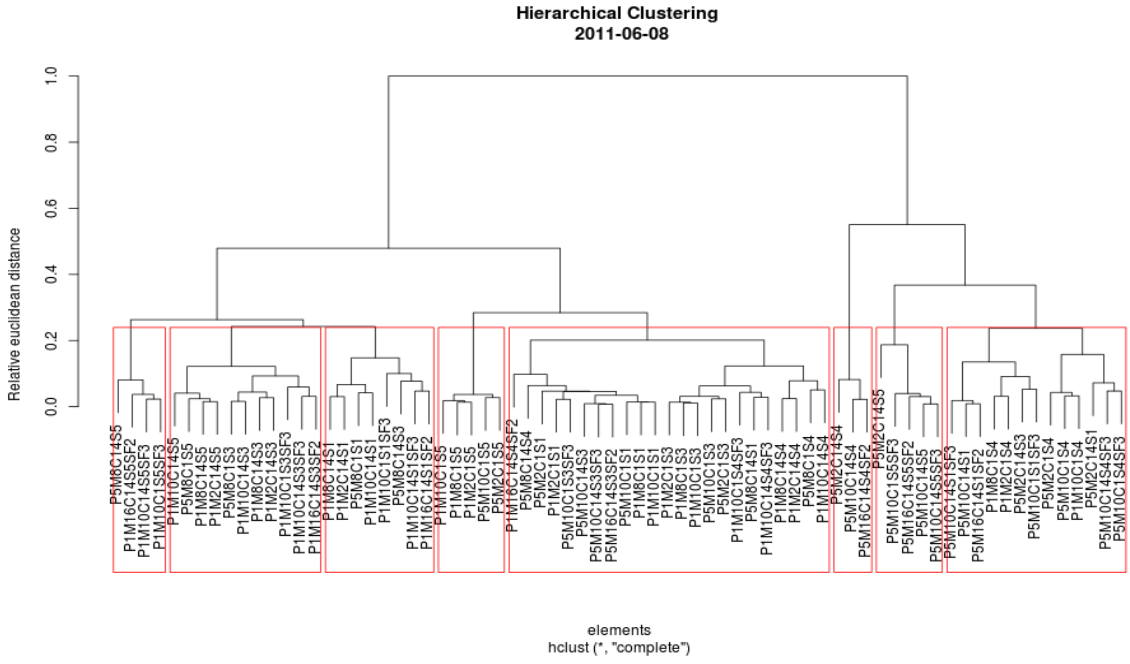

Figure 2. Hierarchical clustering for the global ensemble with 8 clusters for 06/08/2011.

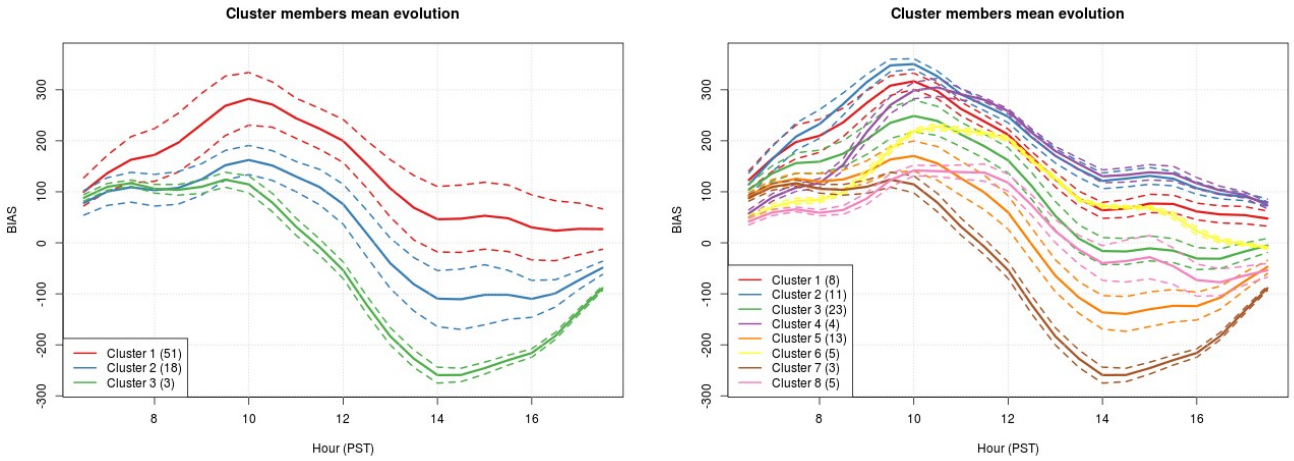

Figure 3. Mean SAW derived BIAS (W m^{-2}) evolution and standard deviation (dashed lines) for 3 clusters (left) and 8 clusters (right) for 06/08/2011. The number in brackets corresponds to the members number per each cluster.

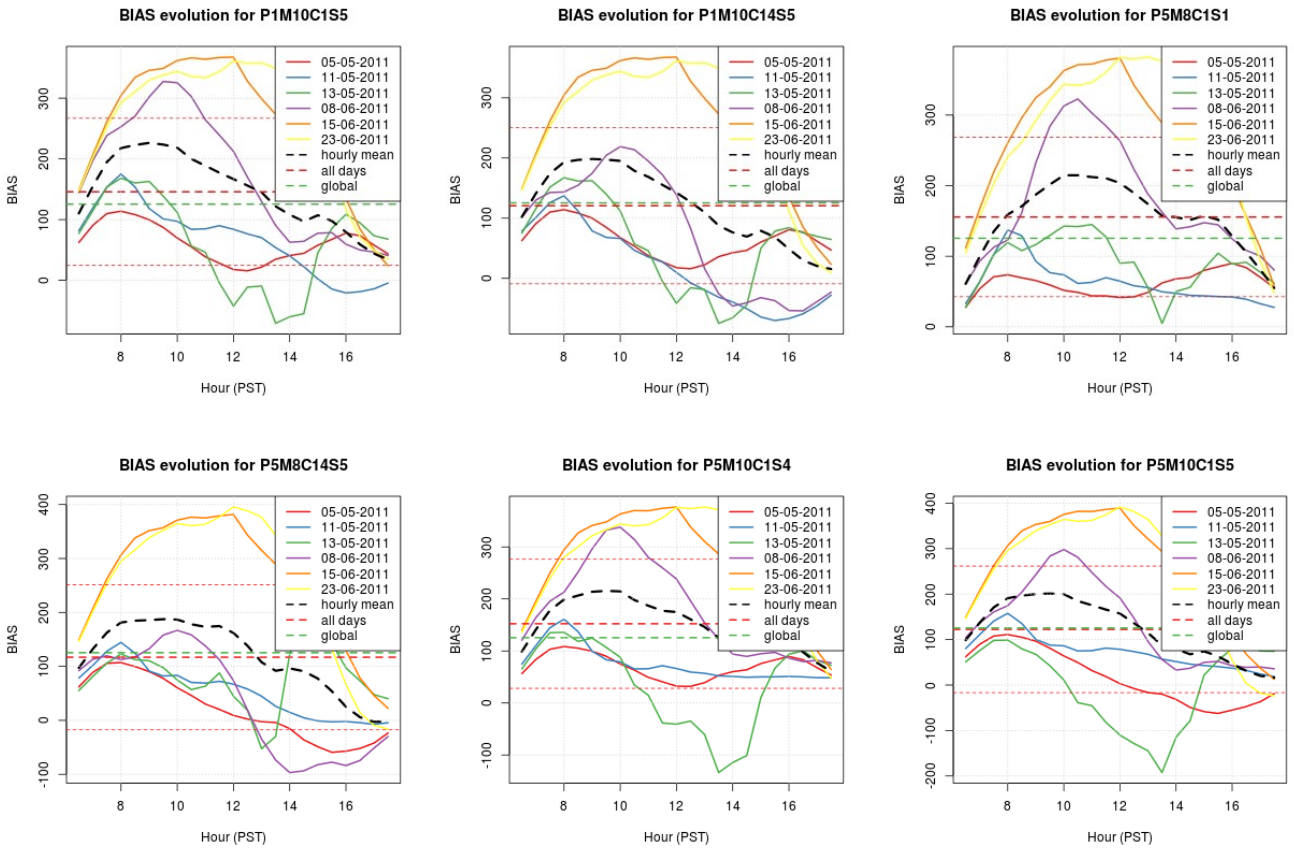

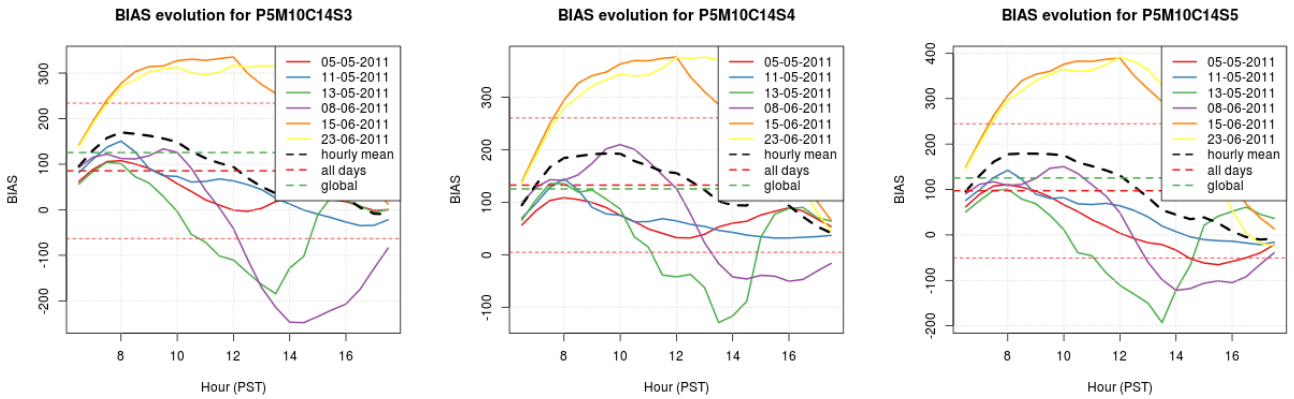

Figure 4. SAW derived BIAS (W m^{-2}) evolution for each model configuration. The "all days" dashed line represents the scheme averaged BIAS and the "global" dashed line represents the all schemes and all days averaged BIAS.

TABLE 2. Selected schemes

Cluster	Model configuration	GHI BIAS behavior
1	P5M8C1S1	positive
2	P1M10C14S5	worst in the morning
3	P5M10C14S3	best in the afternoon
4	P5M8C14S5	positive
5	P5M10C1S4	post meridian (pm) negative
6	P5M10C1S5 P1M10C1S5	positive
7	P5M10C14S4	pm negative (worst in the afternoon)
8	P5M10C14S5	pm negative (best in the morning)

TABLE 3. Weighted BIAS derived from MODIS Cloud Water Path (g m-2)

wBIAS	**20110505 19:00 UTC**	**20110511 18:25 UTC**	**20110513 18:15 UTC**	**20110608 18:50 UTC**	**20110615 18:55 UTC**	**20110623 18:05 UTC**	**mean**
NAM	1.92	12.20	25.11	-27.25	-23.08	19.00	1.32
P5M8C1S1	-1.17	-3.26	180.89	-32.94	-37.23	-41.55	10.79
P5M10C14S3	11.20	3.92	192.51	57.64	-28.03	-33.93	33.89
P1M10C14S5	5.58	3.38	157.55	-10.43	-34.84	-39.70	13.59
P1M10C1S5	5.58	-2.63	156.48	-21.06	-34.84	-39.69	10.64
P5M10C14S5	10.01	1.42	202.81	8.18	-36.36	-41.06	24.17
P5M10C1S5	10.04	-0.20	202.71	-21.25	-36.34	-41.05	18.99
P5M10C1S4	0.996	-2.88	159.99	-25.40	-38.02	-41.26	8.90
P5M10C14S4	0.995	-1.39	160.05	-3.33	-38.02	-41.26	12.84
P5M8C14S5	10.43	1.08	209.99	0.691	-36.87	-41.22	24.02

TABLE 4. Weighted RMSD derived from MODIS Cloud Water Path (g m-2)

wRMSD	**20110505 19:00 UTC**	**20110511 18:25 UTC**	**20110513 18:15 UTC**	**20110608 18:50 UTC**	**20110615 18:55 UTC**	**20110623 18:05 UTC**	**mean**
NAM	6.54	26.96	58.41	48.41	40.96	50.43	38.62
P5M8C1S1	4.24	10.85	337.83	57.16	54.02	59.46	87.26
P5M10C14S3	26.60	9.50	337.17	111.89	43.99	52.39	96.92

P1M10C14S5	16.33	10.57	251.94	54.45	50.77	57.65	73.62
P1M10C1S5	16.33	10.08	249.56	48.49	50.76	57.65	72.15
P5M10C14S5	20.58	6.08	337.71	61.20	52.68	58.85	89.52
P5M10C1S5	20.58	6.31	337.17	48.93	52.66	58.84	87.42
P5M10C1S4	7.83	9.44	283.77	50.59	53.69	59.15	77.41
P5M10C14S4	7.83	6.47	283.36	52.44	53.69	59.15	77.15
P5M8C14S5	24.13	5.74	343.44	56.37	52.08	59.05	90.13

TABLE 5. BIAS and RMSD derived from San Diego (KNKX) radiosonde Temperature (°C) from surface to 3km

	20110506 00:00 UTC		**20110512 00:00 UTC**		**20110514 00:00 UTC**		**20110609 00:00 UTC**		**20110616 00:00 UTC**		**20110624 00:00 UTC**	
P5M8C1S1	-1.10	1.93	-0.68	1.88	-0.02	2.01	-0.75	1.80	-1.33	2.20	-1.66	2.93
P5M10C14S3	-0.93	1.79	-0.84	1.91	-0.52	1.96	-1.21	2.66	-1.25	2.05	-1.50	2.78
P1M10C14S5	-1.06	2.12	-0.93	1.91	-0.20	1.93	-0.97	1.69	-1.45	2.28	-1.88	3.00
P1M10C1S5	-1.06	2.12	-0.93	1.92	0.11	2.10	-0.97	1.71	-1.48	2.32	-1.88	3.01
P5M10C14S5	-1.10	1.84	-0.87	1.92	-0.01	2.07	-0.95	1.92	-1.41	2.18	-1.91	2.92
P5M10C1S5	-1.10	1.84	-0.94	1.99	0.09	1.91	-0.91	1.77	-1.42	2.19	-1.92	2.93
P5M10C1S4	-0.94	1.84	-0.65	1.83	0.10	2.08	-0.72	1.82	-1.20	2.16	-1.52	2.83
P5M10C14S4	-0.94	1.84	-0.70	1.84	-0.15	1.93	-0.72	1.77	-1.19	2.15	-1.52	2.83
P5M8C14S5	-1.10	1.84	-0.88	1.92	-0.24	1.83	-0.93	1.89	-1.41	2.18	-1.90	2.92

TABLE 6. BIAS and RMSD derived from San Diego (KNKX) radiosonde Mixing Ratio (g kg^{-1}) from surface to 3km

	20110506 00:00 UTC		**20110512 00:00 UTC**		**20110514 00:00 UTC**		**20110609 00:00 UTC**		**20110616 00:00 UTC**		**20110624 00:00 UTC**	
P5M8C1S1	0.55	1.47	-0.71	1.14	-0.48	1.29	0.02	0.76	-0.64	0.91	-1.77	2.10
P5M10C14S3	0.32	1.68	-0.70	1.12	-0.40	1.37	-0.04	0.73	-0.63	0.85	-1.73	2.06
P1M10C14S5	0.52	1.87	-0.52	0.81	-0.40	1.25	0.14	0.67	-0.63	0.93	-1.73	2.00
P1M10C1S5	0.52	1.87	-0.35	0.66	-0.55	1.34	0.07	0.69	-0.62	0.92	-1.73	2.00
P5M10C14S5	0.44	1.56	-0.67	1.09	-0.59	1.41	0.01	0.77	-0.65	0.88	-1.70	2.09
P5M10C1S5	0.45	1.56	-0.71	1.14	-0.65	1.36	-0.01	0.76	-0.65	0.87	-1.70	2.09
P5M10C1S4	0.48	1.51	-0.61	1.09	-0.56	1.34	0.02	0.79	-0.57	0.91	-1.66	2.02
P5M10C14S4	0.48	1.51	-0.61	1.08	-0.44	1.26	0.03	0.77	-0.57	0.91	-1.66	2.02
P5M8C14S5	0.45	1.56	-0.66	1.08	-0.51	1.39	0.01	0.78	-0.64	0.87	-1.71	2.09

TABLE 7. Inversion base height difference derived from San Diego radiosounding (m)

	20110506 00:00 UTC	**20110512 00:00 UTC**	**20110514 00:00 UTC**	**20110609 00:00 UTC**	**20110616 00:00 UTC**	**20110624 00:00 UTC**
P5M8C1S1	-23.5	-72.1	83.3	-90.3	105.3	18.2
P5M10C14S3	-55.9	-73.9	-194.8	-97.9	63.6	-19.0
P1M10C14S5	122.7	53.9	-70.5	-43.3	147.4	97.8
P1M10C1S5	122.7	100.5	-69.9	-43.3	147.3	97.8
P5M10C14S5	-55.9	-73.3	-193.9	-139.1	63.5	-89.8
P5M10C1S5	-55.9	-73.8	-220.2	-92.3	63.5	-89.8
P5M10C1S4	-23.4	-72.3	-193.3	-137.8	105.4	18.4
P5M10C14S4	-23.4	-72.6	-165.4	-137.9	105.5	18.4
P5M8C14S5	-56.0	-73.3	-136.6	-138.9	63.6	-89.7